AIAA Aviation Forum and ASCEND co-located Conference Proceedings
21 - 25 July 2025, Las Vegas, Nevada
AIAA AVIATION FORUM AND ASCEND 2025

10.2514/6.2025-3557

Numerical investigation of Tandem Flapped Coflow Jet Wings at Cruise at Low Reynolds Numbers

Jaehyoung Jeon * Anthony Diaz † Yan Ren ‡ Gecheng Zha §
Dept. of Mechanical and Aerospace Engineering
University of Miami, Coral Gables, Florida 33124
E-mail: gzha@miami.edu

Abstract

This study numerically investigates the aerodynamic performance of 3D tandem Flapped CoFlow Jet (FCFJ) wing configurations designed for high lift cruise operations under low Reynolds number conditions representative of the Martian atmosphere. The tandem FCFJ wing system integrates fore and hind FCFJ wings equipped with deflectable flaps, enabling substantial flow turning capabilities to achieve ultra-high cruise lift coefficients while maintaining reasonable aerodynamic efficiency. Optimizing the tandem wing geometric arrangement and investigating wake interference mitigation strategies represent the primary objectives of this research. The study employs an in-house validated 3D Reynolds Averaged Navier-Stokes (RANS) solver with the Spalart-Allmaras (SA) turbulence model, a third-order WENO scheme for inviscid flux calculations, and second-order central differencing for viscous terms in CFD simulations. The comparative analysis reveals that while tandem configurations experience wake interference effects reducing hind wing performance by approximately 7.5%, the system achieves nearly 1.9-fold increase in total lift generation compared to single wing arrangements due to increased wing area. The aerodynamic performance degradation caused by tip vortex in 3D configurations is effectively mitigated by incorporating circular tip caps, providing 6.5% improvement in lift-to-drag ratio. The geometric parametric study demonstrates that FCFJ wings with $\beta = 35$ deflection fundamentally alters wake interaction mechanisms, resulting in minimal sensitivity to stagger distance and vertical gap variations. Furthermore, aspect ratio study reveals a good balance when the fore wing operates at AR 3.33, achieving maximum system corrected aerodynamic efficiency of 6.32. Scaling studies confirm the technology's robustness across different vehicle sizes, maintaining strong performance despite at low Reynolds number. The tandem FCFJ system demonstrates exceptional capability for achieving cruise lift coefficients exceeding 3.4 with corrected aerodynamic efficiency C_L/C_{D_c} of 6.32 and C_L/C_D of 10.88, suitable for Mars atmospheric conditions, establishing a foundation for compact, high-performance aircraft designed for Mars exploration missions.

* Ph.D. Candidate
† Master Student
‡ Postdoc Researcher, Ph.D., AIAA member
§ Professor, ASME Fellow, AIAA associate Fellow

Nomenclature

CFJ	CoFlow jet
$FCFJ$	Flapped CoFlow jet
$AoA(\alpha)$	Angle of attack
LE	Leading Edge
TE	Trailing Edge
U	Flow velocity
P	Pumping power
C_L	Lift coefficient $L/(q_\infty S)$
C_D	Drag coefficient $D/(q_\infty S)$
C_μ	Jet momentum coef. $\dot{m}_j U_j/(q_\infty S)$
Pc	Power coefficient $P/(q_\infty S V_\infty)$
$(C_L/C_D)_c$	CFJ wing corrected aerodynamic efficiency $C_L/(C_D$+Pc)
C_L/C_{D_c}	CFJ wing corrected productivity efficiency $C_L^2/(C_D$+Pc)
DS	Deflected Slipstream
G	Vertical distance between the two wings, gap
R_e	Reynolds number
M	Mach number
S	Planform area of the wing
S_t	Longitudinal separation of the two wings, stagger
T_t	Total temperature
P_t	Total pressure
H_t	Total specific enthalpy
U	Flow velocity
P	Pumping power
Pc	Power coefficient $P/(q_\infty S V_\infty)$
c_p	Constant pressure specific heat
γ	Air specific heats ratio
s	Wing Span length
c	Profile chord
q	Dynamic pressure $0.5\,\rho U^2$
p	Static pressure
ρ	Air density
Γ	Total pressure ratio of CFJ pump
β	Deflection angle
ϵ	Resultant force angle
$\dot{m}$	Mass flow across the pump
$_\infty$	Subscript, stands for free stream
$_j$	Subscript, stands for jet

1 Introduction

The increasing interest in Mars exploration has driven a need for technological advancements to extend the operational range of aerial vehicles on the Martian surface. Mars' unique environment presents

significant challenges for aerial mobility due to its thin atmosphere and varied terrain. To overcome these obstacles, high-performance, efficient aircraft specifically designed for Mars are essential for future missions. Such aircraft could greatly enhance mobility and accessibility, facilitating the exploration of vast Martian landscapes, enabling resource discovery, identifying potential water and ice deposits, detecting methane sources, and providing insights into Martian geological history.

One of the primary challenges in developing aircraft for Mars is achieving ultra-high lift coefficients to minimize vehicle size and weight in the thin Martian atmosphere, which is characterized by low Reynolds numbers and low air density. With an atmospheric density roughly 1% that of Earth's, Mars requires innovative aerodynamic solutions, as traditional Earth-based aircraft designs relying on standard wing interactions for lift are not feasible. This distinct atmospheric characteristic demands a paradigm shift in aerodynamic design to achieve sustained flight performance on Mars. Potential solutions include significantly larger wing areas, higher aspect ratios, reduced wing loading, and novel control surfaces tailored specifically for the Martian environment [1].

In nature, tandem wing configurations are commonly observed in insects such as dragonflies and locusts. These biological systems demonstrate how such configurations can provide enhanced stability and maneuverability while improving aerodynamic efficiency through coordinated wing interactions.

Tandem wing configurations have also gained significant attention in recent aerospace applications, particularly with the advancement of electric vertical takeoff and landing (eVTOL) aircraft for urban air mobility [2]. The primary advantage of tandem wing systems lies in their capability to provide enhanced stability during hover operations through dual lifting surfaces. However, this configuration presents aerodynamic challenges including reduced effective aspect ratio and complex wake interactions, where the wake propagation from the fore wing can seriously decrease the effectiveness and efficiency of the hind wing system. Optimizing the tandem wing configuration to maximize cruise aerodynamic efficiency while maintaining high lift coefficients therefore represents a critical research objective.

In conventional tandem wing designs, the hind wing is typically positioned at an elevated vertical gap relative to the fore wing to mitigate adverse wake interference effects and propeller-wing interactions on overall aerodynamic performance. In this study, the hind wing is initially configured at a higher vertical position relative to the fore wing as shown in Fig. 1 to systematically investigate the aerodynamic impact of geometric parameters. This configuration provides comprehensive reference of how stagger distance and vertical gap variations affect lift coefficients, drag coefficients, and overall system efficiency in tandem wing arrangements.

This study numerically investigates the aerodynamic performance of 3D tandem Flapped CoFlow Jet (FCFJ) wing configurations designed for high lift cruise operations under low Reynolds number conditions representative of the Martian atmosphere. The primary objectives are to optimize the tandem wing geometric arrangement and investigate wake interference mitigation strategies to achieve ultra-high cruise lift coefficients while maintaining reasonable aerodynamic efficiency. The tandem FCFJ wing system integrates fore and hind FCFJ wings equipped with deflectable flaps, enabling substantial flow turning capabilities for Mars exploration missions. The research aims to establish a foundation for compact, high-performance aircraft specifically designed for Mars atmospheric conditions.

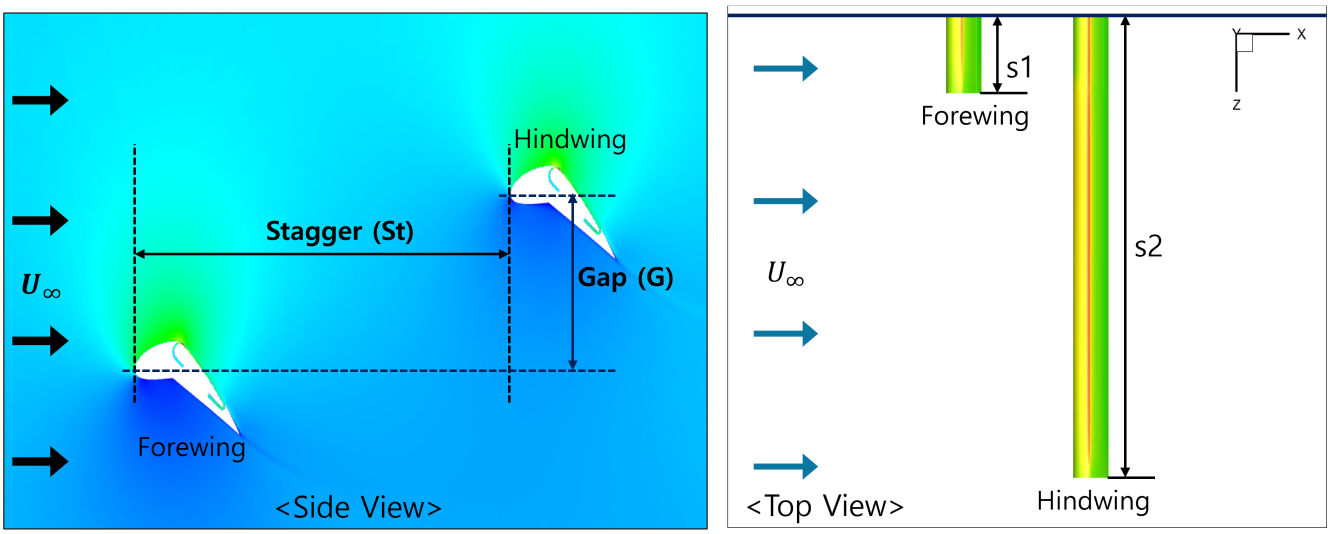

Figure 1: Schematic plot of a tandem FCFJ wing system

1.1 CoFlow Jet (CFJ) Active Flow Control

Active flow control (AFC) has emerged as a promising technology to improve aerodynamic performance, particularly to increase the maximum lift coefficient (C_{Lmax}) by suppressing flow separation and improving airfoil circulation. This is achieved by adding energy to the flow, typically through techniques such as blowing or suction. However, integrating AFC for cruise operation presents a significant challenge. Although the benefits of increased C_{Lmax} are evident, they need to outweigh the energy consumption associated with the AFC system itself for the overall aircraft to achieve a net efficiency gain. One promising AFC technology with the potential to overcome this challenge and improve cruise efficiency is the CoFlow Jet (CFJ) flow control airfoil[3, 4, 5, 6, 7, 8, 9, 10, 11, 12, 13, 14, 15, 16, 17, 18]. This innovative design utilizes a series of small, jet-powered actuators embedded within the airfoil's surface. These actuators inject a high-momentum fluid stream parallel to the main airflow, which effectively energizes the boundary layer and delays flow separation. For a regular CFJ airfoil, as shown in Fig. 2, a small amount of mass flow is drawn into the suction duct, pressurized and powered by a pump, and then injected near the LE tangentially to the main flow. Compared to the 2D baseline airfoil, Wang and Zha[19] show that the 2D CFJ airfoil can achieve a significantly higher cruise lift coefficient and aerodynamic efficiency, defined as

$$(\frac{C_L}{C_D})_c = \frac{C_L}{C_D + P_c} \tag{1}$$

While CoFlow Jet (CFJ) technology offers promising avenues for enhancing cruise performance, it is crucial to evaluate its impact on overall aircraft efficiency. This necessitates consideration of the CFJ power requirement, denoted by the CFJ required power coefficient, Pc. Studies have shown that CFJ wings can maintain high cruise lift coefficient(C_L) even for three-dimensional wings with finite aspect ratios. However, this improved lift performance comes at the cost of reduced aerodynamic efficiency, which can potentially decrease to the level of conventional baseline wings, as reported by Wang et al. [20]. To comprehensively assess the transportation productivity of aircraft, a parameter encompassing both range and gross weight is introduced: cruise productivity efficiency. This metric, proposed by Yang et al. [14], provides a more holistic evaluation of aircraft performance, considering not just aerodynamic

efficiency but also payload capacity and range capability.

$$(\frac{C_L^2}{C_D})_c = \frac{C_L^2}{(C_D + Pc)} \tag{2}$$

CFJ wing can have substantially higher cruise C_L and thus greater productivity efficiency as well. Taking advantage of the CFJ wing high cruise lift coefficient and thus high suction effect on wing upper surface, Ren and Zha [21] design a tandem wing aircraft configuration that the front wing tip vortex is captured by the rear wing to enhance the overall system efficiency. However, for cruise condition, the regular CFJ configuration as shown in Fig. 2 appears to have rapid energy consumption increase when C_L is greater than 1.6[14, 22]. Even though the aerodynamic drag coefficient C_D can remain small and the pure aerodynamic lift-to-drag ratio C_L/C_D can still be very high, the corrected aerodynamic efficiency defined in Eq. (1) can decrease quickly with the increasing C_L.

Flapped CoFlow Jet technology has emerged as a promising solution for achieving high C_L while maintaining acceptable $(C_L/C_D)_c$. This capability makes it particularly relevant for aircraft operating in low-density environments, such as at high altitudes on Earth or in the Martian atmosphere. As demonstrated in previous studies[23, 24], flapped CFJs can significantly enhance lift performance, opening opportunities for various mission applications. Notably, a 2D flapped CFJ study [25] achieved a remarkable $(C_L/C_D)_c$ of 20.5 while simultaneously maintaining a high C_L of 3.74 at a Mach number of 0.26 and a Reynolds number of 1.42×10^5. This demonstrates the potential of flapped CFJ technology for significantly improving aerodynamic performance. Building upon these promising findings, the present study delves into the numerical analysis of 3D flapped CFJs under low Reynolds number conditions, specifically those encountered in low-density environments. This analysis aims to further elucidate the characteristics and potential benefits of this technology for various aeronautical applications, including high-altitude Earth missions and future Martian exploration efforts.

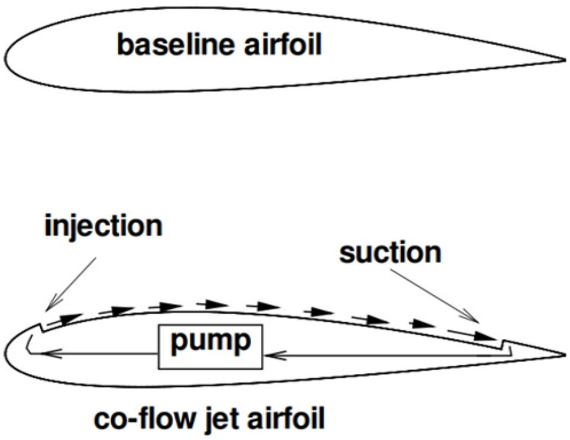

Figure 2: Sketch of CoFlow Jet wing

1.2 Flapped CoFlow Jet Airfoil

The concept of flapped coflow jet airfoil is adopted from the CFJ airfoil with deflected slipstream for VTOL aircraft [26]. It is also guided by the CoFlow jet flow separation mechanism study of Xu and Zha

[27].

The CFJ is applied inside a long flap that is a part of the flapped CFJ airfoil, as shown in Fig.3 [23], which has the injection located at the shoulder of the flap. The regular CFJ airfoil applies the injection very close to the leading edge at a point of around 2-4% Chord location. By deflecting the flap rather than rotating the front of the airfoil, the FCFJ airfoil has the advantage of allowing the airfoil to change the angle of attack and lift coefficient without tilting the wings or the aircraft. The purpose of this paper is to numerically demonstrate that the coflow jet is feasible to deflect the slipstream of a propeller by an airfoil with a simple plain flap at low energy expenditure. This will lay a foundation for further development of the DS-CFJ technology at low Reynolds number.

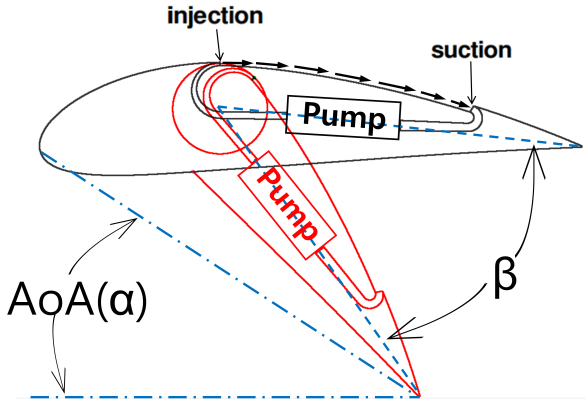

Figure 3: Sketch of flapped CFJ airfoil with the CoFlow jet applied on the flap

2 Methodology

2.1 Lift and Drag Calculation

The momentum and pressure at the injection and suction slots produce a reactionary force, which is automatically measured by the force balance in wind tunnel testing. However, for CFD simulation, the full reactionary force needs to be included. Using control volume analysis, the reactionary force can be calculated using the flow parameters at the injection and suction slot opening surfaces. Zha et al. [4] give the following formulations to calculate the lift and drag due to the jet reactionary force for a CFJ airfoil. By considering the effects of injection and suction jets on the CFJ airfoil, the expressions for these reactionary forces are given as :

$$F_{x_{cfj}} = (\dot{m}_j V_{j1} + p_{j1} A_{j1}) * cos(\theta_1 - \alpha) - (\dot{m}_j V_{j2} + p_{j2} A_{j2}) * cos(\theta_2 + \alpha) \tag{3}$$

$$F_{y_{cfj}} = (\dot{m}_{j1} V_{j1} + p_{j1} A_{j1}) * sin(\theta_1 - \alpha) + (\dot{m}_{j2} V_{j2} + p_{j2} A_{j2}) * sin(\theta_2 + \alpha) \tag{4}$$

where the subscripts 1 and 2 stand for the injection and suction respectively, and θ_1 and θ_2 are the angles between the injection and suction slot's surface and a line normal to the airfoil chord. α is the angle of attack.

The total lift and drag on the airfoil can then be expressed as:

$$D = R'_x - F_{x_{cfj}} \tag{5}$$

$$L = R'_y - F_{y_{cfj}} \tag{6}$$

where R'_x and R'_y are the surface integral of pressure and shear stress in the x (drag) and y (lift) directions excluding the internal ducts of injection and suction. For CFJ wing simulations, the total lift and drag are calculated by integrating Eqs.(5) and (6) in the spanwise direction.

2.2 Jet Momentum Coefficient

The jet momentum coefficient C_μ is a parameter used to quantify the jet intensity. It is defined as:

$$C_\mu = \frac{\dot{m} V_j}{\frac{1}{2}\rho_\infty {V_\infty}^2 S} \tag{7}$$

where $\dot{m}$ is the injection mass flow, V_j is the mass-averaged injection velocity, ρ_∞ and V_∞ denote the free stream density and velocity, and S is the planform area.

2.3 Micro-compressor Power Coefficient

CFJ is implemented by mounting a pumping system inside the wing that withdraws air from the suction slot and blows it into the injection slot. The power consumption is determined by the jet mass flow and total enthalpy change as the following:

$$P = \dot{m}(H_{t1} - H_{t2}) \tag{8}$$

where H_{t1} and H_{t2} are the mass-averaged total enthalpy in the injection cavity and suction cavity respectively, P is the Power required by the pump and $\dot{m}$ the jet mass flow rate. Introducing P_{t1} and P_{t2} the mass-averaged total pressure in the injection and suction cavity respectively, the compressor efficiency η, and the total pressure ratio of the pump $\Gamma = \frac{P_{t1}}{P_{t2}}$, the power consumption is expressed as:

$$P = \frac{\dot{m} C_p T_{t2}}{\eta}(\Gamma^{\frac{\gamma-1}{\gamma}} - 1) \tag{9}$$

where γ is the specific heat ratio equal to 1.4 for air. The power coefficient is expressed as:

$$P_c = \frac{P}{\frac{1}{2}\rho_\infty V_\infty^3 S} \tag{10}$$

2.4 Aerodynamic Efficiency

The conventional wing aerodynamic efficiency is defined as:

$$\frac{C_L}{C_D} \tag{11}$$

For the CFJ wing, the ratio above still represents the pure aerodynamic relationship between lift coefficient and drag coefficient. However since CFJ active flow control consumes energy, the ratio above is modified to take into account the energy consumption of the micro-compressor. The formulation of the corrected aerodynamic efficiency for CFJ wings is:

$$(\frac{C_L}{C_D})_c = \frac{C_L}{C_D + P_c} \tag{12}$$

where P_c is the micro-compressor power coefficient defined in Eqn. 10 and C_L and C_D are the lift and drag coefficients of the CFJ wing. If the micro-compressor power coefficient is set to 0, this formulation returns to the aerodynamic efficiency of a conventional airfoil.

This study involves a tandem wing configuration. For example, the coefficient of lift for each wing can be defined individually as:

$$C_{L1} = \frac{L_1}{\frac{1}{2}\rho_\infty V_\infty^2 S_1}, \quad C_{L2} = \frac{L_2}{\frac{1}{2}\rho_\infty V_\infty^2 S_2} \tag{13}$$

where the subscript 1 and 2 stand for the first and second wing. For the aircraft system with tandem wings, the system lift coefficient is defined as the total lift based on the total wing area below:

$$C_{Lt} = \frac{L_1 + L_2}{\frac{1}{2}\rho_\infty V_\infty^2 (S_1 + S_2)} \tag{14}$$

where the subscript t stands for tandem wing.

Substituting Eq. 13 to Eq. 14, the system lift coefficient can be expressed as:

$$C_{Lt} = \frac{C_{L1}S_1 + C_{L2}S_2}{S_1 + S_2} \tag{15}$$

Eq. 15 is actually the same as the area weighted lift coefficient. Similarly, the coefficient of system drag and CFJ power can be defined as:

$$C_{Dt} = \frac{C_{D1}S_1 + C_{D2}S_2}{S_1 + S_2} \tag{16}$$

$$P_{ct} = \frac{P_1 S_1 + P_2 S_2}{S_1 + S_2} \tag{17}$$

The corrected drag coefficient is:

$$(C_{Dc})_t = C_{Dt} + P_{ct} \tag{18}$$

The aerodynamic efficiency and the productivity efficiency of the tandem wing system then can be defined following the same way as Eq. 12. To see the relations clearly, we take the aerodynamic efficiency of the tandem wing as an example below:

$$\left(\frac{L}{D_c}\right)_t = \frac{L_1 + L_2}{D_1 + D_2 + P_1/V_\infty + P_2/V_\infty} = \frac{C_{Lt}\frac{1}{2}\rho_\infty V_\infty^2(S_1+S_2)}{C_{Dt}\frac{1}{2}\rho_\infty V_\infty^2(S_1+S_2) + P_{ct}\frac{1}{2}\rho_\infty V_\infty^2(S_1+S_2)} = \frac{S_1C_{L1} + S_2C_{L2}}{S_1C_{D1} + S_2C_{D2} + S_1P_1 + S_2P_2} \tag{19}$$

That is:

$$\left(\frac{L}{D_c}\right)_t = \frac{C_{Lt}}{(C_{Dc})_t} \tag{20}$$

2.5 CFD Simulation Setup

The FASIP(Flow-Acoustics-Structure Interaction Package) CFD code is used to conduct the numerical simulation. The 3D Reynolds Averaged Navier-Stokes (RANS) equations with one-equation Spalart-Allmaras(SA) turbulence model is used. A 3rd order WENO scheme for the inviscid flux [28, 29, 30, 31, 32, 33] and a 2nd order central differencing for the viscous terms [28, 32] are employed to discretize the Navier-Stokes equations. The low diffusion E-CUSP scheme used as the approximate Riemann solver suggested by Zha et al [29] is utilized with the WENO scheme to evaluate the inviscid fluxes. Implicit time marching method using Gauss-Seidel line relaxation is used to achieve a fast convergence rate [34]. Parallel computing is implemented to save wall clock simulation time [35].

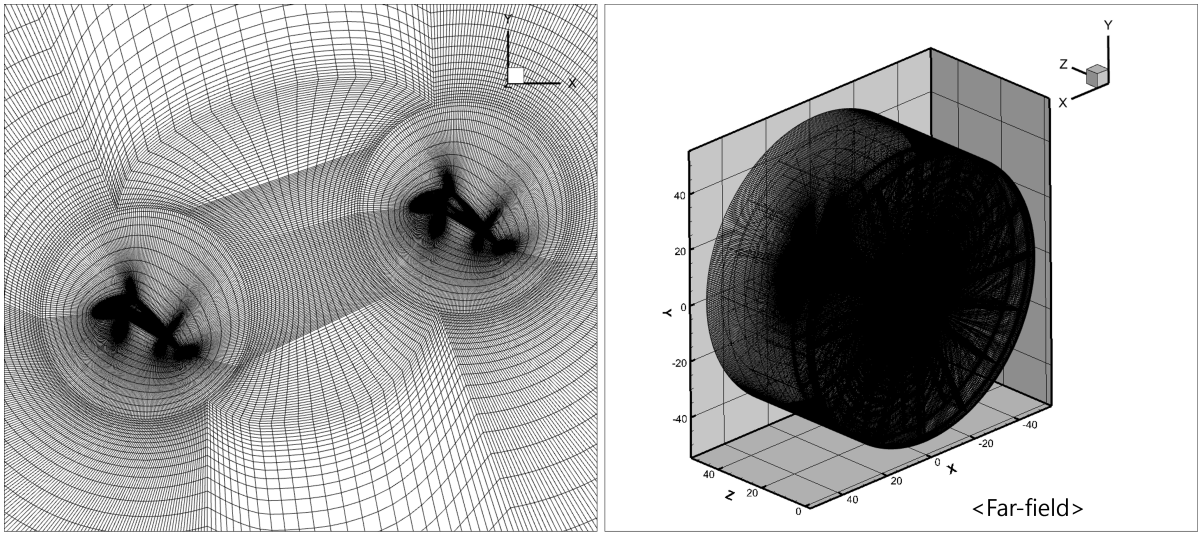

Figure 4: Mesh for the tandem FCFJ wing

2.6 Boundary Conditions

The 3rd order accuracy no slip condition is enforced on the solid surface with the wall treatment suggested in [36] to achieve the flux conservation on the wall. The far field boundary is located at 50 chord with a O-mesh topology. The computational mesh is shown in Fig. 4. Total pressure, total temperature and flow angles are specified at the upstream portion of the far field. Constant static pressure is applied at the downstream portion of the far field. The first grid point on the wing surface is placed at $y^+ \approx 1$.

The atmospheric properties for Mars, relevant to the present analysis, are summarized in Table 1.

Table 1: Flow Conditions and Properties

Variable	**Value**	**Unit**
p	655	[Pa]
T	220	[K]
ρ	0.01576	[kg/m^3]
μ	1.11E-05	[kg/m s]
R	188.9	[J/kg K]
L_{ref}	1	[m]
U_∞	39.53	[m/s]
γ	1.3	
M_∞	0.17	
Re_∞	5.63E+04	

3 Results and Discussion

3.1 Comparison between Single Wing and Tandem Wing

The single wing study is conducted in [37], and among the cases examined, we focus on the one with $\beta = 35°$, an injection size of $0.6\%C$, and an aspect ratio (AR) of 20 at C_μ 0.13 for comparison. The single wing and each of the tandem wings have the same aspect ratio of 20. Figure 5 illustrates the Mach contour of the single wing, whereas Figure 6 presents that of the tandem wing configuration. In the tandem wing configuration, the hind wing is positioned at $S_t = 3C$ and $G = 1C$, representing a typical geometric arrangement for investigating wake interference effects.

In both configurations, the flow remains well attached to the wing surfaces; however, it becomes evident that the upstream flow conditions over the hind wing in the tandem arrangement are significantly influenced by the wake propagation from the fore wing. This wake interference creates a complex flow environment that directly affects the aerodynamic performance of the downstream hind wing. Figure 7 shows the pressure coefficient (C_p) distribution at span 50%, where the tandem hind wing exhibits a markedly different profile compared to the isolated single wing case. The C_p distribution from the leading edge to the CFJ injection location demonstrates consistently lower values, indicating reduced suction on the upper surface of the hind wing. This altered pressure distribution results in a lift coefficient (C_L) that is approximately 7.5% lower than that of the single FCFJ wing, as documented in Table 2. It should be noted that the aerodynamic coefficients for each individual component (fore wing and hind wing) are calculated based on their respective single wing planform areas in Eq. 13, while the total system values are computed using the weighted area of both wings in Eq. 19.

Notably, the drag coefficient (C_D) of the hind wing increases significantly due to the modified flow conditions in the wake region, leading to a substantial decrease in overall aerodynamic efficiency. The pure aerodynamic lift-to-drag ratio (C_L/C_D) decreases by approximately 32% to 9.19, while the corrected aerodynamic efficiency (C_L/C_{D_c}) that accounts for CFJ power consumption decreases by about 22% to 5.79. These reductions in efficiency highlight the aerodynamic penalties associated with wake interference effects in tandem wing configurations. The wake from the fore wing creates altered velocity and pressure fields that degrade the inlet conditions for the hind wing, resulting in reduced suction on the upper

surface and increased drag. Despite these efficiency losses, utilizing wings of the same planform area in a tandem arrangement allows for an approximate 1.9-fold increase in total system lift, demonstrating the potential benefits of this configuration for applications requiring high lift coefficients.

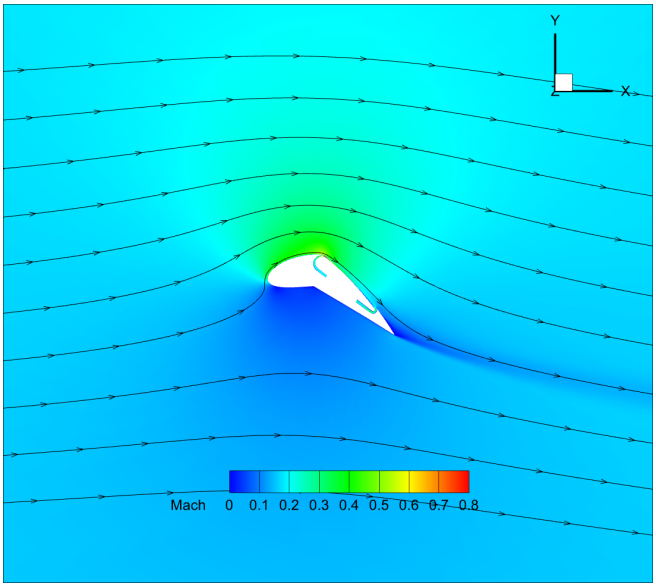

Figure 5: Mach contour of Single FCFJ wing

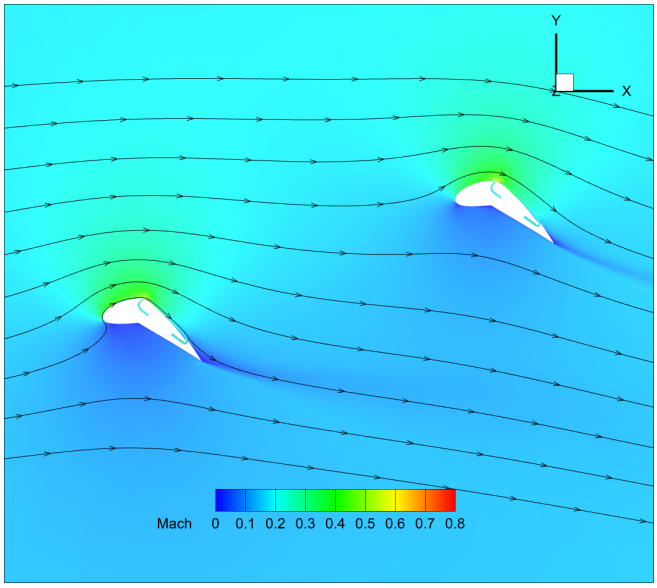

Figure 6: Mach contour of Tandem FCFJ wing

Table 2: Aerodynamic Performance Comparison for Single and Tandem Configurations: $\beta = 35°$, AR=20, injection size=0.6%C

Single FCFJ Wing

	C_μ	C_L	C_D	P_c	C_L/C_D	$C_L/(C_D+P_c)$	$C_L^2/(C_D+P_c)$
	0.13	3.53	0.26	0.21	13.4	7.44	26.27

Tandem FCFJ Wing

Part	C_μ	C_L	C_D	P_c	C_L/C_D	$C_L/(C_D+P_c)$	$C_L^2/(C_D+P_c)$
ForeWing	0.13	3.47	0.10	0.21	35.13	11.17	38.72
HindWing	0.14	3.27	0.63	0.22	5.15	3.83	12.52
Total		3.37	0.37	0.22	9.19	5.79	19.49

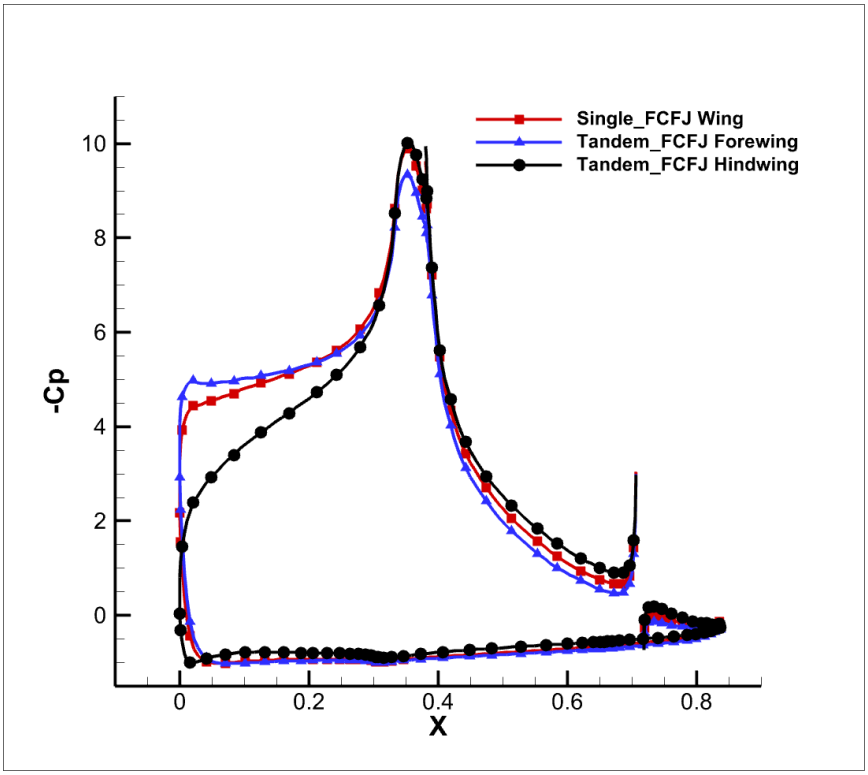

Figure 7: Comparison of Cp distribution

3.2 Effect of Tip Cap

In a three-dimensional configuration, aerodynamic performance is significantly reduced due to strong tip vortices that develop at the wing tips. These tip vortices create induced drag and reduce the effective lift generation, particularly affecting the performance of finite aspect ratio wings. To mitigate this issue and improve overall aerodynamic efficiency, the use of a tip cap is considered. The cap is designed with a circular planform shape and a diameter of $2C$, providing an effective barrier to reduce tip vortex formation and spillage flow around the wing tips. For the tip cap study, the aspect ratio of each of the tandem wings remains the same as 20. The Mach contours with and without the tip cap are shown in Figures 8 and 9, respectively, illustrating the flow field differences in the tip region. The presence of the tip cap clearly reduces the flow spillage around the wing tips and modifies the local flow patterns.

Figures 10 and 11 illustrate the pressure coefficient (C_p) distribution at 50% span for both configurations. For both the fore wing and hind wing, the C_p distributions remain nearly identical regardless of the presence of the cap, indicating that the mid-span flow characteristics are not significantly affected by the tip treatment. This suggests that the tip cap influence is primarily localized to the tip region without adversely affecting the inboard aerodynamic performance.

However, at 95% span, as shown in Figures 12 and 13, the presence of the cap notably influences the aerodynamic performance near the tip region. The tip cap effectively reduces the pressure equalization between the upper and lower surfaces, maintaining higher suction on the upper surface and thereby improving lift generation near the tips. This improvement results in enhanced overall system performance, with the tip cap configuration achieving an increase of approximately 6.5% in the lift-to-drag ratio

(C_L/C_D) to 9.18 and over 5% in the corrected aerodynamic efficiency (C_L/C_{D_c}) to 5.92, as summarized in Table 3. These performance improvements demonstrate the effectiveness of the tip cap in reducing three-dimensional losses associated with tip vortex.

Given the consistent performance benefits observed across the tandem wing system, all subsequent studies employ the same tip cap configuration to ensure optimal aerodynamic efficiency.

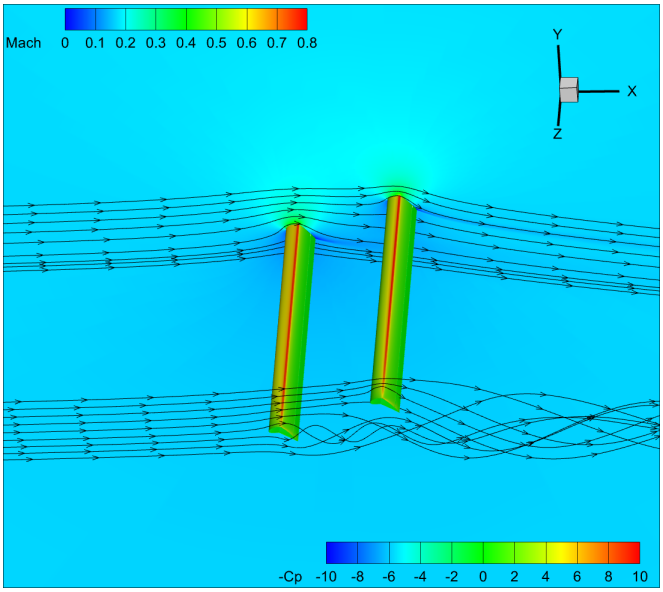

Figure 8: Mach contour without tip cap

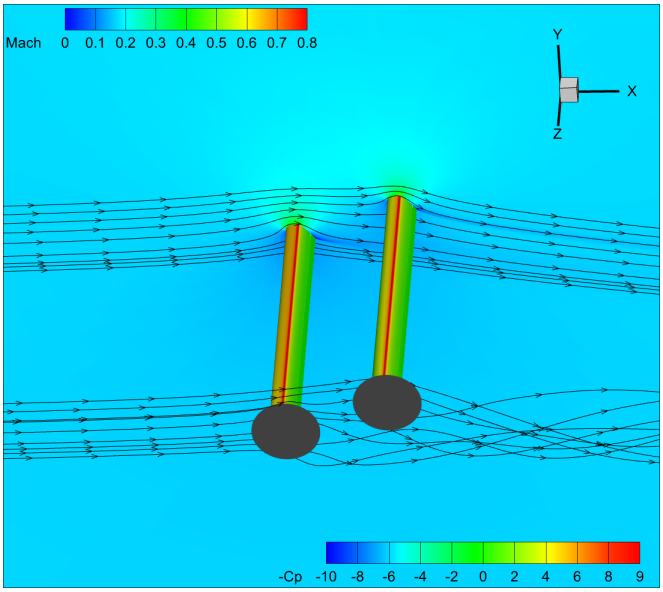

Figure 9: Mach contour with tip cap

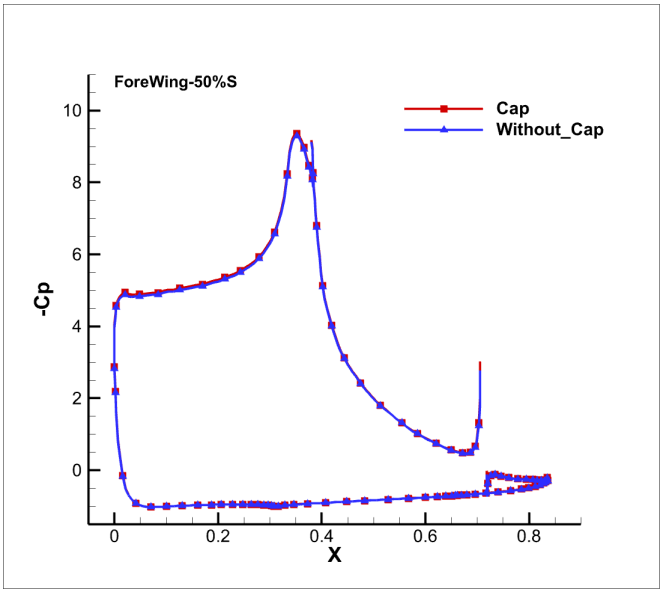

Figure 10: C_p distribution for Forewing at 50%s

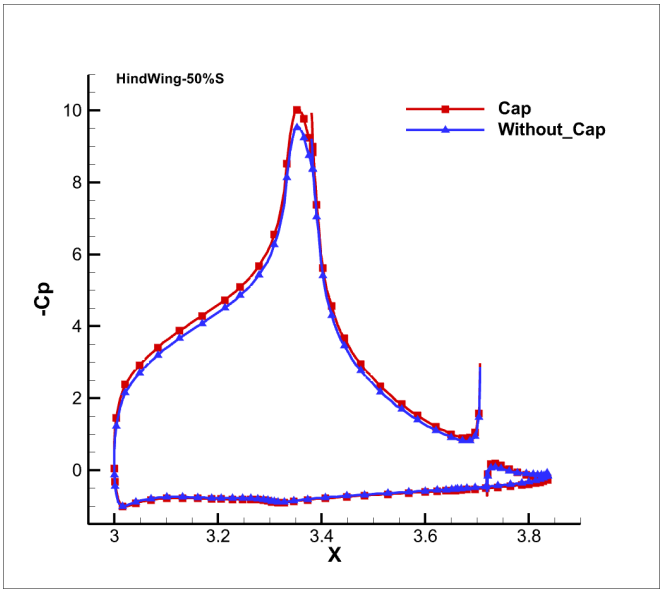

Figure 11: C_p distribution for Hindwing at 50%s

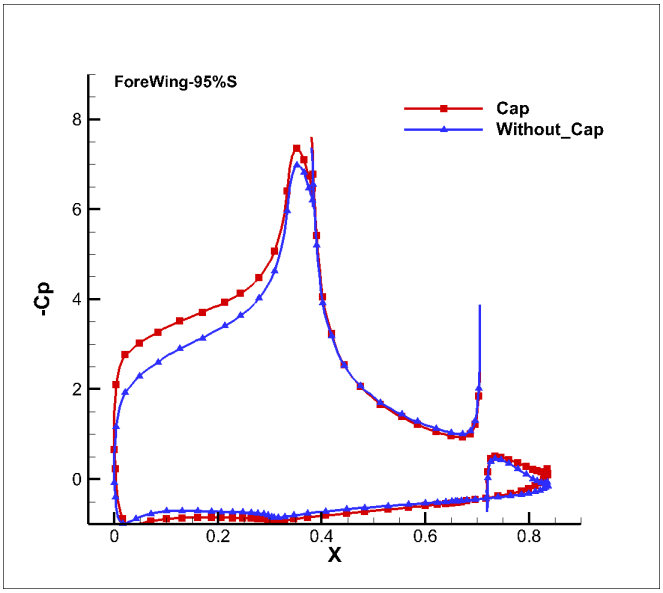

Figure 12: C_p distribution for Forewing at 95%s

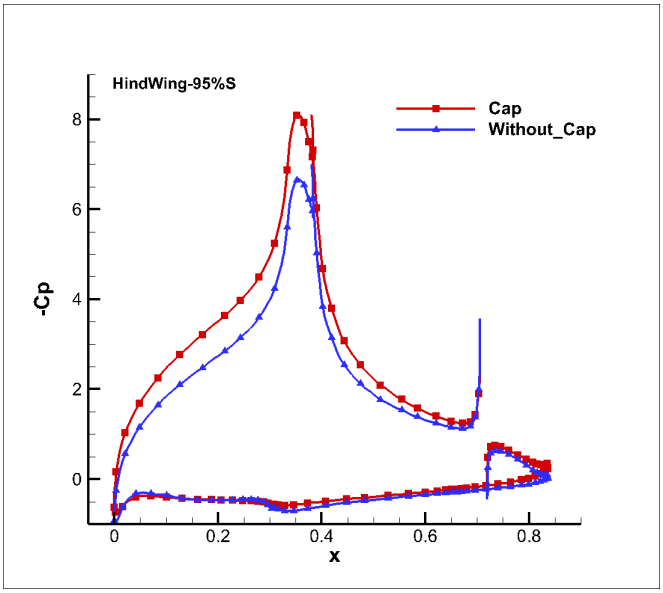

Figure 13: C_p distribution for Hindwing at 95%s

Table 3: Aerodynamic Performance Comparison for without tip cap and with tip cap: $\beta = 35°$, AR=20, C_t=3, G=1, injection size=0.6%C, Forewing C_μ=0.13, Hindwing C_μ=0.14

Without Cap						
Part	C_L	C_D	P_c	C_L/C_D	$C_L/(C_D+P_c)$	C_L^2/C_{Dc}
ForeWing	3.41	0.14	0.21	24.89	9.86	33.58
HindWing	3.01	0.61	0.18	4.91	3.79	11.40
Total	3.21	0.38	0.19	8.55	5.63	18.06

With Cap						
Part	C_L	C_D	P_c	C_L/C_D	$C_L/(C_D+P_c)$	C_L^2/C_{Dc}
ForeWing	3.47	0.11	0.21	32.07	10.84	37.57
HindWing	3.08	0.61	0.18	5.10	3.92	12.10
Total	3.28	0.36	0.20	9.18	5.92	19.40

3.3 Stagger and Gap effects

The geometric parametric study results presented in Table 4 demonstrate that the influence of stagger distance (S_t) and vertical gap (G) on aerodynamic performance is relatively modest when operating at a deflection angle of $\beta = 35°$. In this study, the fore airfoil has an aspect ratio of 20, while the hind airfoil has an aspect ratio of 13.33. The corrected aerodynamic efficiency (C_L/C_{D_c}) of the total system shows small variation across the tested configurations, ranging from 5.93 to 5.98, representing less than 1% difference between the cases. This relatively small sensitivity to geometric parameters contrasts significantly with the behavior observed in conventional tandem wing configurations.

In conventional tandem wing systems without active flow control, the wake propagation from the fore wing typically creates substantial wake interference effects that severely degrade the performance of the

hind wing. The wake maintains its horizontal trajectory and directly impinges on the hind wing's upper surface, causing significant velocity deficits and pressure field disturbances that result in reduced lift generation and increased drag coefficients. However, FCFJ configuration with $\beta = 35°$ deflection angle fundamentally alters this wake interaction mechanism. The substantial flow turning capability of the FCFJ directs the wake flow significantly downward, effectively redirecting the wake trajectory away from the hind wing's upper surface. By redirecting the airflow downward, this approach effectively reduces the usual direct wake interference issues found in traditional tandem wing setups.

The total pressure contours presented in Figures 14 and 15 clearly illustrate this phenomenon, showing how the fore wing wake is deflected well below the hind wing's operational region. The wake from the fore wing with FCFJ maintains its downward trajectory due to the strong flow turning effects of the CFJ system, thereby preserving the incoming flow quality for the hind wing. This explains the relatively stable performance characteristics observed across different S_t and G configurations, as the hind wing operates in essentially undisturbed freestream conditions rather than in the degraded wake environment typical of conventional tandem arrangements. This finding suggests that FCFJ technology offers significant advantages for tandem wing configurations by mitigating the traditional wake interference penalties, allowing for more flexible geometric arrangements without substantial performance degradation.

Table 4: Aerodynamic Performance Comparison for Various Geometric Configurations: $\beta = 35°$, injection size=0.6%C, Forewing AR=20 with C_μ=0.13, Hindwing AR=13.33 with C_μ=0.14

Part	S_t	G	C_L	C_D	P_c	C_L/C_D	C_L/C_{D_c}	C_L^2/C_{D_c}
ForeWing	3	1	3.48	0.15	0.21	23.78	9.70	33.79
HindWing			3.17	0.64	0.22	4.92	3.66	11.62
Total			3.36	0.35	0.22	9.72	5.98	20.08
ForeWing	2.4	0.2	3.54	0.14	0.21	25.63	10.06	35.64
HindWing			3.03	0.65	0.22	4.64	3.46	10.47
Total			3.34	0.34	0.22	9.69	5.94	19.83
ForeWing	2.4	0	3.57	0.10	0.22	34.57	11.19	39.94
HindWing			2.88	0.69	0.22	4.19	3.17	9.14
Total			3.30	0.34	0.22	9.78	5.93	19.55

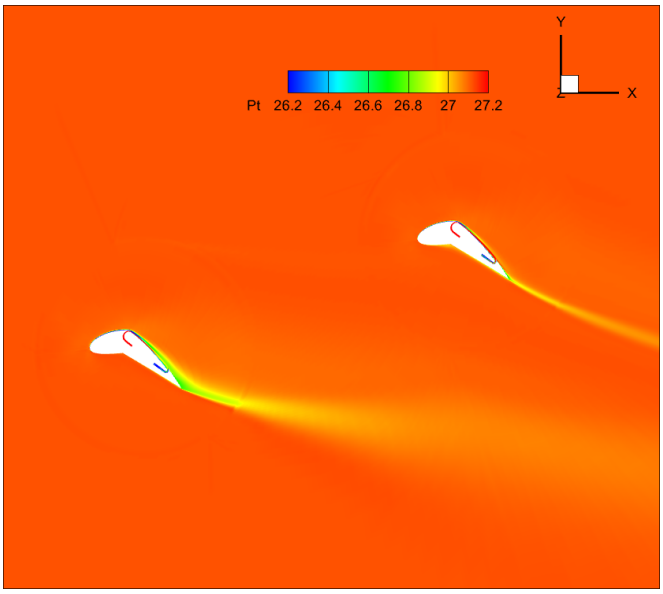

Figure 14: Total pressure plot for S_t=3 with G=1

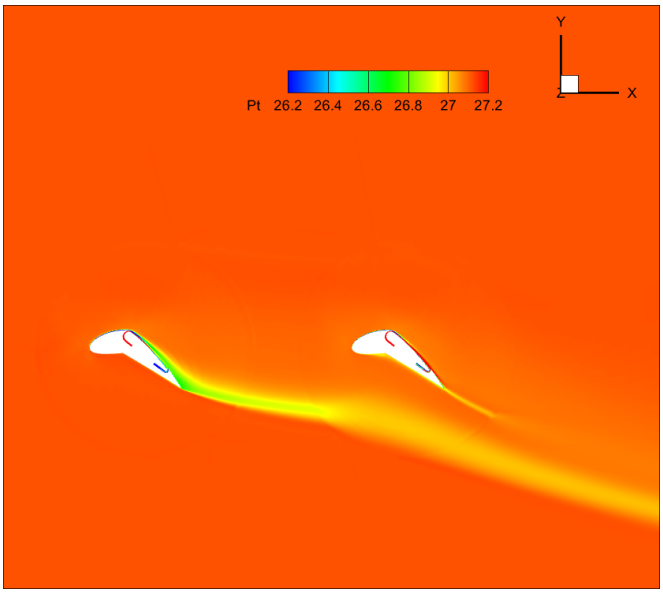

Figure 15: Total pressure plot for S_t=2.4 with G=0

3.4 Effect of Aspect Ratio (AR)

This study examines how the aspect ratio (AR) combination between the fore wing and hind wing affects the overall aerodynamic performance of the tandem configuration. Understanding the interaction between different aspect ratios is crucial for optimizing tandem wing systems, as the wake characteristics from the fore wing directly influence the performance of the downstream hind wing. In this parametric analysis, the hind wing's AR remains constant at 20, while the fore wing's AR is systematically adjusted to values of 3.33 (1/6), 6.67 (1/3), and 13.33 (2/3) relative to that of the hind wing. This range of aspect ratios allows for comprehensive evaluation of the wake interference effects and their impact on system performance. The findings are presented in Table 5 with St=3, and G=1. For the tandem wing system, the total aspect ratio is defined as the area-weighted average of the individual wing aspect ratios. This approach accounts for the relative contribution of each wing component based on their respective planform areas. The total aspect ratio can be expressed as:

$$AR_t = \frac{AR_1 \times S_1 + AR_2 \times S_2}{S_1 + S_2} \tag{21}$$

where AR_1 and AR_2 are the aspect ratios of the fore wing and hind wing respectively, and S_1 and S_2 are their corresponding planform areas. This formulation ensures that wings with larger planform areas have proportionally greater influence on the overall system aspect ratio, providing a representative metric for the tandem wing configuration's geometric characteristics. The total performance in Table 5 is calculated based on area average of the tandem wings [21].

As the aspect ratio (AR) of the fore wing increases, there is a consistent enhancement in both the lift coefficient (C_L) and the corrected aerodynamic efficiency (C_L/C_{D_c}) for the fore wing itself. Higher aspect ratios reduce the relative influence of tip effects and improve the spanwise lift distribution, leading to better aerodynamic performance for the fore wing. Conversely, the aerodynamic performance of the hind wing experiences a notable decline as the fore wing AR increases. This degradation occurs because higher

aspect ratio fore wings generate stronger wake structures that persist further downstream, creating more severe wake interference effects.

Specifically, an increase in the fore wing's AR leads to a sharp rise in the drag coefficient (C_D) of the hind wing, which directly contributes to a lower overall corrected aerodynamic efficiency (C_L/C_{D_c}). The wake from higher aspect ratio fore wings maintains its intensity over longer distances, resulting in more significant velocity deficits and pressure field disturbances that adversely affect the hind wing's inlet conditions. The total system C_L/C_{D_c} achieves its peak value of 6.32 when the fore wing AR is 3.33, representing an optimal balance between fore wing performance and wake interference effects. However, this efficiency drops by approximately 8.4% to 5.79 when the fore wing AR reaches 20, indicating diminishing returns from further aspect ratio increases.

This study demonstrates that with an increase in the aspect ratio of the fore wing, its influence on the flow field over the hind wing becomes stronger, resulting in a considerable decline in the hind wing's aerodynamic efficiency. The wake interference effects become stronger and more persistent, creating a trade-off between individual wing performance and system-level efficiency. Additional parametric studies are required to develop methods to mitigate these adverse wake interference effects while maximizing overall system aerodynamic efficiency, potentially through optimized geometric arrangements or active flow control strategies.

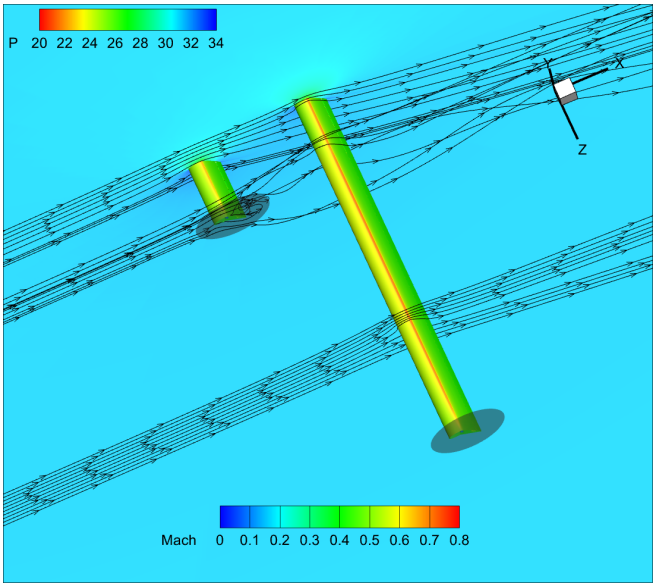

Figure 16: Flow field for AR 3.33 (Fore wing) with AR20 (Hind wing)

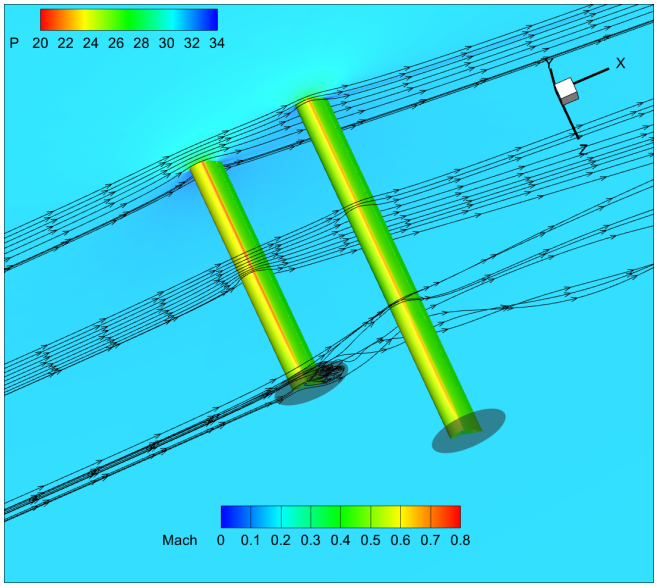

Figure 17: Flow field for AR 13.33 (Fore wing) with AR20 (Hind wing)

Table 5: Aerodynamic Performance Comparison for Various AR Configurations: $\beta = 35°$, S_t=3, G=1, injection size=0.6%C, Forewing C_μ=0.13, Hindwing C_μ=0.14

Part	AR	C_L	C_D	P_c	C_L/C_D	$C_L/(C_D + P_c)$	$C_L^2/(C_D + P_c)$
ForeWing	3.33	2.72	0.39	0.22	6.89	4.42	12.00
HindWing	20	3.56	0.30	0.23	11.74	6.69	23.83
Total	17.62	3.44	0.32	0.23	10.88	6.32	21.76
ForeWing	6.66	3.14	0.26	0.22	11.87	6.50	20.44
HindWing	20	3.53	0.36	0.23	9.71	5.92	20.89
Total	16.67	3.43	0.34	0.23	10.13	6.05	20.75
ForeWing	13.33	3.36	0.14	0.21	24.39	9.56	32.14
HindWing	20	3.39	0.50	0.22	6.80	4.69	15.91
Total	17.33	3.38	0.35	0.22	9.54	5.88	19.88
ForeWing	20	3.47	0.10	0.21	35.13	11.17	38.72
HindWing	20	3.27	0.63	0.22	5.15	3.83	12.52
Total	20	3.37	0.37	0.22	9.19	5.79	19.49

3.5 Reynolds number effect with scaled configuration

The scaled configuration study results presented in Table 6 examine the aerodynamic performance when both the aircraft fuselage and wing dimensions are reduced to approximately 70% of the reference size. This scaling investigation is crucial for understanding how the FCFJ tandem wing system performs under different vehicle size constraints, which directly affects the operating Reynolds number and overall aerodynamic characteristics. The scaling from the reference configuration ($S_t = 3$, $G = 1$, $Re = 5.63 \times 10^4$) to the reduced size configuration ($S_t = 2.1$, $G = 0.7$, $Re = 3.94 \times 10^4$) maintains the same relative geometric proportions while operating at a lower Reynolds number regime. The Reynolds number reduction of approximately 30% reflects the combined effects of reduced characteristic length and the low-density Martian atmospheric conditions.

Despite the significant scale reduction and corresponding Reynolds number decrease, the aerodynamic performance degradation remains relatively modest. The total system corrected aerodynamic efficiency (C_L/C_{D_c}) decreases from 5.98 to 5.50, representing an 8% reduction in efficiency. This small penalty is attributed to the CFJ AFC that triggers the boundary layer transition from laminar to turbulent even with the Reynolds reduced by 30%. The lift coefficient analysis reveals that the FCFJ system maintains strong lift generation capability despite the scale reduction. The total system lift coefficient decreases modestly from 3.36 to 3.26, representing only a 3% reduction. Individual wing performance shows that the fore wing maintains excellent lift generation with C_L of 3.48 and 3.37 for the reference and scaled configurations, respectively, while the hind wing achieves C_L of 3.17 and 3.09. These cruise lift coefficients remain exceptionally high for conventional wing standards, demonstrating the effectiveness of the FCFJ flow control in maintaining strong circulation enhancement even at reduced scales and lower Reynolds numbers.

The relatively modest performance degradation with scale reduction indicates that the FCFJ tandem

wing concept maintains its effectiveness even when scaled down to smaller vehicle sizes. This finding is particularly significant for Mars exploration applications where vehicle weight and size constraints may necessitate compact aircraft designs. The maintained high lift coefficients and acceptable efficiency characteristics suggest that the FCFJ technology can be successfully implemented across a range of vehicle scales while preserving both the lift generation capability and aerodynamic efficiency levels required for Mars atmospheric conditions.

Table 6: Aerodynamic Performance Comparison for Scaled Configuration:
$\beta = 35°$, injection size=0.6%C, Forewing AR=20 with C_μ=0.13, Hindwing AR=13.33 with C_μ=0.14

Part	Chord	S_t	G	Re	C_L	C_D	P_c	C_L/C_D	C_L/C_{D_c}	C_L^2/C_{D_c}
ForeWing	1	3	1	5.63E+04	3.48	0.15	0.21	23.78	9.70	33.79
HindWing					3.17	0.64	0.22	4.92	3.66	11.62
Total					3.36	0.35	0.22	9.72	5.98	20.08
ForeWing	0.7	2.1	0.7	3.94E+04	3.37	0.15	0.25	22.11	8.41	28.36
HindWing					3.09	0.62	0.26	4.97	3.52	10.88
Total					3.26	0.34	0.25	9.58	5.50	17.95

4 Conclusion

This paper presents a comprehensive numerical investigation of tandem Flapped CoFlow Jet (FCFJ) wing configurations designed for high lift cruise operations under low Reynolds number conditions representative of the Martian atmosphere. The study demonstrates the potential of FCFJ technology to overcome the fundamental aerodynamic challenges associated with flight in Mars' thin atmospheric environment.

The comparative analysis between single and tandem FCFJ configurations reveals that while the tandem arrangement experiences wake interference effects that reduce individual hind wing performance by approximately 7.5% in lift coefficient, the system achieves nearly 1.9-fold increase in total lift generation due to increased wing area. The tandem configuration maintains a corrected aerodynamic efficiency (C_L/C_{D_c}) of 5.79 and achieves remarkable total system lift coefficients exceeding 3.37, demonstrating the viability of this approach for high-lift cruise at low Reynolds number.

The implementation of tip caps proves highly effective in mitigating three-dimensional losses, providing a 6.5% improvement in aerodynamic efficiency and over 5% enhancement in corrected efficiency. This modification increases the system C_L/C_{D_c} from 5.63 to 5.92, highlighting the importance of tip treatment in finite aspect ratio tandem configurations.

The geometric parametric study reveals that FCFJ technology fundamentally alters traditional tandem wing wake interaction mechanisms. The substantial flow deflection capability at $\beta = 35$ redirects the fore wing wake significantly downward, minimizing wake interference effects on the hind wing. This results in low sensitivity to stagger distance and vertical gap variations, with system efficiency varying by less than 1% across the tested configurations, contrasting sharply with conventional tandem arrangements.

The aspect ratio investigation demonstrates an optimal balance between individual wing performance and wake interference effects when the fore wing operates at AR 3.33, achieving the highest system

C_L/C_{D_c} of 6.32. Higher fore wing aspect ratios, while improving individual performance, create stronger wake structures that adversely affect hind wing efficiency, resulting in diminishing system-level returns.

The scaling study confirms the robustness of FCFJ technology across different vehicle sizes. Despite a 30% Reynolds number reduction corresponding to 70% scale reduction, the system maintains strong performance with only 8% efficiency degradation and 3% lift coefficient reduction attributed to CFJ AFC triggering boundary layer transition from laminar to turbulent. The scaled configuration achieves C_L values of 3.26 and C_L/C_{D_c} of 5.50, demonstrating the technology's adaptability to various aircraft size constraints.

Overall, the tandem FCFJ wing system demonstrates exceptional capability for achieving ultra-high cruise lift coefficients exceeding 3.3 while maintaining reasonable corrected aerodynamic efficiency of C_L/C_{D_c} 6.32 and C_L/C_D 10.88. suitable for Mars atmospheric conditions. The productivity efficiency (C_L^2/C_{D_c}) values reaching 21.76 indicate significant potential for payload and range optimization. This investigation establishes a solid foundation for developing compact, high-performance aircraft specifically designed for Mars exploration missions, potentially revolutionizing aerial mobility on the Martian surface through dramatically reduced aircraft size and weight requirements while enabling increased range and payload capabilities.

5 Acknowledgment

The teaching assistantship support from the University of Miami is acknowledged.

Disclosure: The University of Miami and Dr. Gecheng Zha may receive royalties for future commercialization of the intellectual property used in this study. The University of Miami is also equity owner in CoFlow Jet, LLC, licensee of the intellectual property used in this study.

References

[1] Koji FUJITA, Remi LUONG, Hiroki NAGAI, Keisuke ASAI, "Conceptual Design of Mars Airplane," *Trans. JSASS Aerospace Tech. Japan, Vol.10, No.ists28, pp.5-10*, 2012.

[2] K. R. Antcliff, S. K. Whiteside, L. W. Kohlman, and C. Silva, "Baseline Assumptions and Future Research Areas for Urban Air Mobility Vehicles," *AIAA Paper 2019-0528, AIAA SciTech 2019 Forum, San Diego, CA*, January 2019. 7-11 January 2019.

[3] G.-C. Zha and D. C. Paxton, "A Novel Flow Control Method for Airfoil Performance Enhancement Using Co-Flow Jet." *Applications of Circulation Control Technologies*, Chapter 10, p. 293-314, Vol. 214, Progress in Astronautics and Aeronautics, AIAA Book Series, Editors: Joslin, R. D. and Jones, G.S., 2006.

[4] G.-C. Zha, W. Gao, and C. Paxton, "Jet Effects on Co-Flow Jet Airfoil Performance," *AIAA Journal, No. 6,*, vol. 45, pp. 1222–1231, 2007.

[5] G.-C. Zha, C. Paxton, A. Conley, A. Wells, and B. Carroll, "Effect of Injection Slot Size on High Performance Co-Flow Jet Airfoil," *AIAA Journal of Aircraft*, vol. 43, 2006.

[6] G.-C. Zha, B. Carroll, C. Paxton, A. Conley, and A. Wells, "High Performance Airfoil with Co-Flow Jet Flow Control," *AIAA Journal*, vol. 45, 2007.

[7] Wang, B.-Y. and Haddoukessouni, B. and Levy, J. and Zha, G.-C., "Numerical Investigations of Injection Slot Size Effect on the Performance of Co-Flow Jet Airfoil," *Journal of Aircraft*, vol. Vol. 45, No. 6,, pp. pp.2084–2091, 2008.

[8] B. P. E. Dano, D. Kirk, and G.-C. Zha, "Experimental Investigation of Jet Mixing Mechanism of Co- Flow Jet Airfoil." AIAA-2010-4421, 5th AIAA Flow Control Conference, Chicago, IL, 28 Jun - 1 Jul 2010.

[9] B. P. E. Dano, G.-C. Zha, and M. Castillo, "Experimental Study of Co-Flow Jet Airfoil Performance Enhancement Using Micro Discreet Jets." AIAA Paper 2011-0941, 49th AIAA Aerospace Sciences Meeting, Orlando, FL, 4-7 January 2011.

[10] A. Lefebvre, B. Dano, W. Bartow, M. Fronzo, and G. Zha, "Performance and energy expenditure of coflow jet airfoil with variation of mach number," *Journal of Aircraft*, vol. 53, no. 6, pp. 1757–1767, 2016.

[11] A. Lefebvre, G-C. Zha, "Numerical Simulation of Pitching Airfoil Performance Enhancement Using Co-Flow Jet Flow Control," *AIAA paper 2013-2517*, June 2013.

[12] A. Lefebvre, G-C. Zha, "Cow-Flow Jet Airfoil Trade Study Part I : Energy Consumption and Aerodynamic Performance," *Proceedings of the AIAA Flow Control Conference*, June 2014.

[13] A. Lefebvre, G-C. Zha, "Cow-Flow Jet Airfoil Trade Study Part II : Moment and Drag," *Proceedings of the AIAA Flow Control Conference*, June 2014.

[14] Yunchao Yang, Gecheng Zha, "Super-Lift Coefficient of Active Flow Control Airfoil: What is the Limit?," *AIAA Paper 2017-1693, AIAA SCITECH2017, 55th AIAA Aerospace Science Meeting, Grapevine, Texas, 9-13 January 2017*, 2017.

[15] Gecheng Zha, Yunchao Yang, Yan Ren, Brendan McBreen, "Super-Lift and Thrusting Airfoil of Coflow Jet Actuated by Micro-Compressors," *AIAA Paper-2018-3061, AIAA AVIATION Forum 2018, Flow Control Conference, June 25-29*, 2018.

[16] Lefebvre, A. and Zha, G.-C., "Trade Study of 3D Co-Flow Jet Wing for Cruise Performance." AIAA Paper 2016-0570, AIAA SCITECH2016, AIAA Aerospace Science Meeting, San Diego, CA, 4-8 January 2016.

[17] Kewei Xu, Gecheng Zha, "High Control Authority 3D Aircraft Control Surfaces Using Co-Flow Jet," *AIAA Journal of Aircraft*, 2020.

[18] Kewei Xu, Yan Ren, Gecheng Zha, "Numerical Analysis of Energy Expenditure for Co-Flow Wall Jet Separation Control," *AIAA Journal, published online: 11 Jan 2022, doi.org/10.2514/1.J061015*, 2022.

[19] Yang Wang and Gecheng Zha, "Study of Mach Number Effect for 2D Co-Flow Jet Airfoil at Cruise Conditions," *AIAA Paper 2019-3169, AIAA Aviation 2019 Forum, 17-21 June 2019, Dallas, Texas*, 2019.

[20] Yang Wang and Gecheng Zha, "Study of Mach Number Effect for 3D Co-Flow Jet Wings at Cruise Conditions," *AIAA Paper 2020-0045, AIAA SciTech Forum, 6-10 January 2020, Orlando, FL*, 2020.

[21] Yan Ren, Gecheng Zha, "Performance Enhancement by Tandem Wings Interaction of CoFlow Jet Aircraft," *AIAA Paper 2021-1823, AIAA SciTech Forum, 11–15; 19–21 January 2021, VIRTUAL EVENT*, 2021.

[22] Yang Wang, Yunchao Yang and Gecheng Zha, "Study of Super-Lift Coefficient of Co-Flow Jet Airfoil and Its Power Consumption," *AIAA Paper 2019-3652, AIAA Aviation 2019 Forum, 17-21 June 2019, Dallas, Texas* , 2019.

[23] Jaehyoung Jeon, Yan Ren, and Gecheng Zha, "Toward Ultra-High Cruise Lift Coefficient Using Flapped CoFlow Jet Airfoil," *AIAA SciTech Forum, January 23-27*, 2023.

[24] Jaehyoung Jeon, Brendan McBreen, Yan Ren, and Gecheng Zha, "Study of 3D Flapped CoFlow Jet Wings for Ultra-High Cruise Lift Coefficient," *AIAA Aviation Forum, June 12-16*, 2023.

[25] Jaehyoung Jeon, Yan Ren, and Gecheng Zha, "Flapped CoFlow Jet Airfoil for High Lift Cruise at Low Reynolds Number in Martian Atmosphere," *AIAA SciTech Forum, January 8-12*, 2024.

[26] Zha, G.-C,, "Feasibility Study of Deflected Slipstream Airfoil for VTOL Hover Enabled by CoFlow Jet," *Proceedings of AIAA Aviation Forum 2023, 12–16 June 2023, San Diego, CA*, 2023.

[27] Kewei Xu, Yan Ren, and Gecheng Zha, "Separation Control by Co-Flow Wall Jet," *AIAA Paper 2021-2946, AIAA AVIATION Forum, August 2-6*, 2021.

[28] Y.-Q. Shen and G.-C. Zha, "Large Eddy Simulation Using a New Set of Sixth Order Schemes for Compressible Viscous Terms ," *Journal of Computational Physics*, vol. 229, pp. 8296–8312, 2010.

[29] Zha, G.C., Shen, Y.Q. and Wang, B.Y., "An improved low diffusion E-CUSP upwind scheme ," *Journal of Computer and Fluids*, vol. 48, pp. 214–220, Sep. 2011.

[30] Y.-Q. Shen and G.-Z. Zha , "Generalized finite compact difference scheme for shock/complex flowfield interaction," *Journal of Computational Physics*, vol. doi:10.1016/j.jcp.2011.01.039, 2011.

[31] Shen, Y.-Q. and Zha, G.-C. and Wang, B.-Y., " Improvement of Stability and Accuracy of Implicit WENO Scheme," *AIAA Journal*, vol. 47, No. 2, pp. 331–344, 2009.

[32] Shen, Y.-Q. and Zha, G.-C. and Chen, X.-Y., " High Order Conservative Differencing for Viscous Terms and the Application to Vortex-Induced Vibration Flows," *Journal of Computational Physics*, vol. 228(2), pp. 8283–8300, 2009.

[33] Shen, Y.-Q. and Zha, G.-C. , " Improvement of the WENO Scheme Smoothness Estimator," *International Journal for Numerical Methods in Fluids*, vol. DOI:10.1002/fld.2186, 2009.

[34] G.-C. Zha and E. Bilgen, "Numerical Study of Three-Dimensional Transonic Flows Using Unfactored Upwind-Relaxation Sweeping Algorithm," *Journal of Computational Physics*, vol. 125, pp. 425–433, 1996.

[35] B.-Y. Wang and G.-C. Zha, "A General Sub-Domain Boundary Mapping Procedure For Structured Grid CFD Parallel Computation," *AIAA Journal of Aerospace Computing, Information, and Communication*, vol. 5, No.11, pp. 2084–2091, 2008.

[36] Y.-Q. Shen, G.-C. Zha, and B.-Y. Wang, "Improvement of Stability and Accuracy of Implicit WENO Scheme ," *AIAA Journal*, vol. 47, pp. 331–344, 2009.

[37] Jaehyoung Jeon, Yan Ren, and Gecheng Zha, "Flapped CoFlow Jet Wing for High Lift Cruise in the Martian Atmosphere," *AIAA Aviation Forum, July 29- August 2*, 2024.